

## *International Journal of Scientific Research and Reviews*

### **Quantum Computational, Experimental Vibrational Spectroscopic and Molecular Docking Investigation of 4-Oxo-4H-Chromone-3-Carboxaldehyde**

**R. Madivanane<sup>1</sup> and A.Harikrishnan<sup>2\*</sup>**

<sup>1</sup>Associate Professor, Bharathidasan Govt. College for Women, Puducherry, India.

<sup>2\*</sup>Research scholar, Barathiar University, Coimbatore, Tamilnadu, India.

#### **ABSTRACT**

In this present work, the theoretical vibrational frequencies of 4-oxo-4H-chromone-3-carboxaldehyde have been calculated by HF and DFT (B3LYP) methods with the basis set 6-311G++ (d, p) and the experimental FT-IR and FT-Raman spectra of the title molecule is also recorded in the region 4000 - 400  $\text{cm}^{-1}$ . The calculated vibrational frequencies are compared with the experimentally observed spectra and a detailed assignment of the vibrational spectra of the titled molecule is carried out. The HOMO-LUMO, Natural Bonding Orbital and Molecular Electrostatic Potential analysis of the titled compound have been performed to understand the charge transfer, conjugative interaction, nucleophilic, electrophilic reactive sites and hydrogen bonding interaction in the molecule system. Drug likeness, the drug bioavailability and molecular docking study of the investigated compound have also been performed. The titled compound possess a better binding affinity with residues of TRP 89 A, ARG 82A, THR 90A, LEU 86A, GLY87 A, ILE88A, GLUA 33, PRO A34, PHE123A by making hydrogen bonds  $\pi$ - $\pi$  and  $\pi$ - $\sigma$  interactions. This result reveals that, the existence of an unsaturated reactive aldehyde at the C-3 position can react as acceptor and it seems to be accountable for various biological activities and provides a profound knowledge about the design of the drug related with this target protein in the pharmaceutical industry.

**KEYWORDS:** FT-Raman; FT-IR; HOMO- LUMO; MEP; NBO.

#### **\*Corresponding Author**

**A. Harikrishnan**

Research scholar, Barathiar University,

No.26. Madha kovil street,

Nellithoppe, Puducherry-600 005

E Mail - [krish53hari80@gmail.com](mailto:krish53hari80@gmail.com)

## **INTRODUCTION**

Biological activity mainly depends upon on the molecular structure and hence the relationship between molecular structure and biological activity can be understood with the knowledge of the complete vibrational spectrum. Chromone is the parent compound of flavonoids which imbibes oxygen naturally and is found in normal human diet<sup>1</sup>. Most of the natural and synthetic chromone derivatives have found wide range of biological application<sup>2</sup>. The title compound 4-oxo-4H-chromone-3-carboxaldehyde also known as 3-Formylchromone(3FC)with chemical formula C<sub>10</sub>H<sub>6</sub>O<sub>3</sub> is a benzo- -pyrone, substituted by an aldehyde group in the position C-3. The 3FC is plays the significant role in various chemical reactions as reduction, oxidation, radical nucleophilic addition, many types of annulations, cycloaddition reactions and shows an assorted building block in synthesis of heterocycles compound<sup>3-4</sup>. Depending on the nature of the functional group present at the position three, the 3FC is a versatile synthons for the synthesis of a variety of novel heterocyclic derivatives possessing diverse biological applications such as antifungal, anti-viral, anti-microbial, anti-allergenic, anti-inflammatory and anticancer<sup>5</sup>. Due to its wide range of chemical and biological application of the titled compound, a detailed quantum computational and vibrational spectroscopic study is required in current research. Even though a partial analysis of the 3FC is carried out by Agnieszka Dziejulska-Kulaczowska etal<sup>6</sup>, the lack of complete vibrational analysis of the titled compound can lead to an experimental FTIR, FT-Raman spectral analysis along with quantum computational study for thorough understanding of the investigated molecule. In this the present work, the optimized molecular structure of the titled molecule is computed by HF and DFT method. The theoretically calculated IR, Raman spectra are compared with the experimentally observed vibrational spectra using FT-IR and FT-Raman techniques and the detailed assignment of the vibrational spectra are assigned. The Frontier molecular orbital (FMO), Molecular electrostatic potential (MEP) and Thermo dynamic properties of the 3FC are also presented and discussed at the DFT level. Also, in order to validate the biological activity of the chosen compound, molecular docking study is carried out on the optimized structure of 3FC to understand the binding mechanism with target proteins which is related with promoting cell proliferation, tumor development in epidermis and apoptosis activity.

## MATERIALS AND METHOD

### *Computational details*

A quantum computational calculations of the 3FC was carried out by 6-311G++(d,p) basis set including 'd' polarization function on heavy atoms and 'p' polarization functions on hydrogen atoms at the framework of HF and DFT methods using version 8 of Gaussian 09W programme package<sup>7</sup>. The theoretical IR and Raman spectra were simulated using Gabedit version 2.4.5<sup>8</sup> with band width of  $10\text{cm}^{-1}$ . The calculated vibrational wave numbers have been scaled using multiple scaling factors in order to get a good agreement with those of the experimental ones and to offset the systematic error caused by neglecting anharmonicity<sup>9</sup>. The ground state optimized structure of the 3FC molecule is presented in Fig.1. For the optimized structure, the bond parameters such as bond length and bond angle are calculated and a good correlation observed in comparisons with available literature. In order to predict the inhibitory activity of the title compound, computer aided molecular docking studies were performed by using AutoDock (version 4.2)<sup>10</sup>.

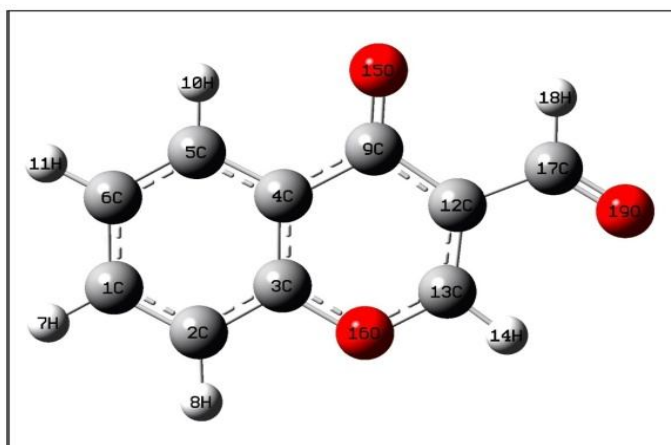


**Fig.1: Optimized molecular structure of 3FC.**

### *Experimental Details*

The investigated compound 3FC is an off-white crystalline powder with a melting point of  $160^{\circ}\text{C}$  was obtained in solid form from M/s Sigma chemicals, which posses 98% of purity and the sample is subjected to record FTIR and FTR spectra without any further purification. The room temperature Fourier transform infrared spectrum of the title compound was recorded in  $4000 - 400\text{cm}^{-1}$  region at a resolution of  $2\text{cm}^{-1}$  using Bruker IFS-66 Fourier transform spectrometer using the KBr pellet technique. The FT-Raman spectrum of the chosen compound, 3FC was recorded in the region  $3500$  and  $50\text{cm}^{-1}$  on the same instrument equipped with an FRA-106 FT-Raman accessories with  $1.064\text{nm}$  excitation from an Nd: YAG laser. The theoretically computed and experimentally

recorded FTIR and FT-Raman spectra of the investigated compound are shown in Fig. 2 and Fig-3 respectively.

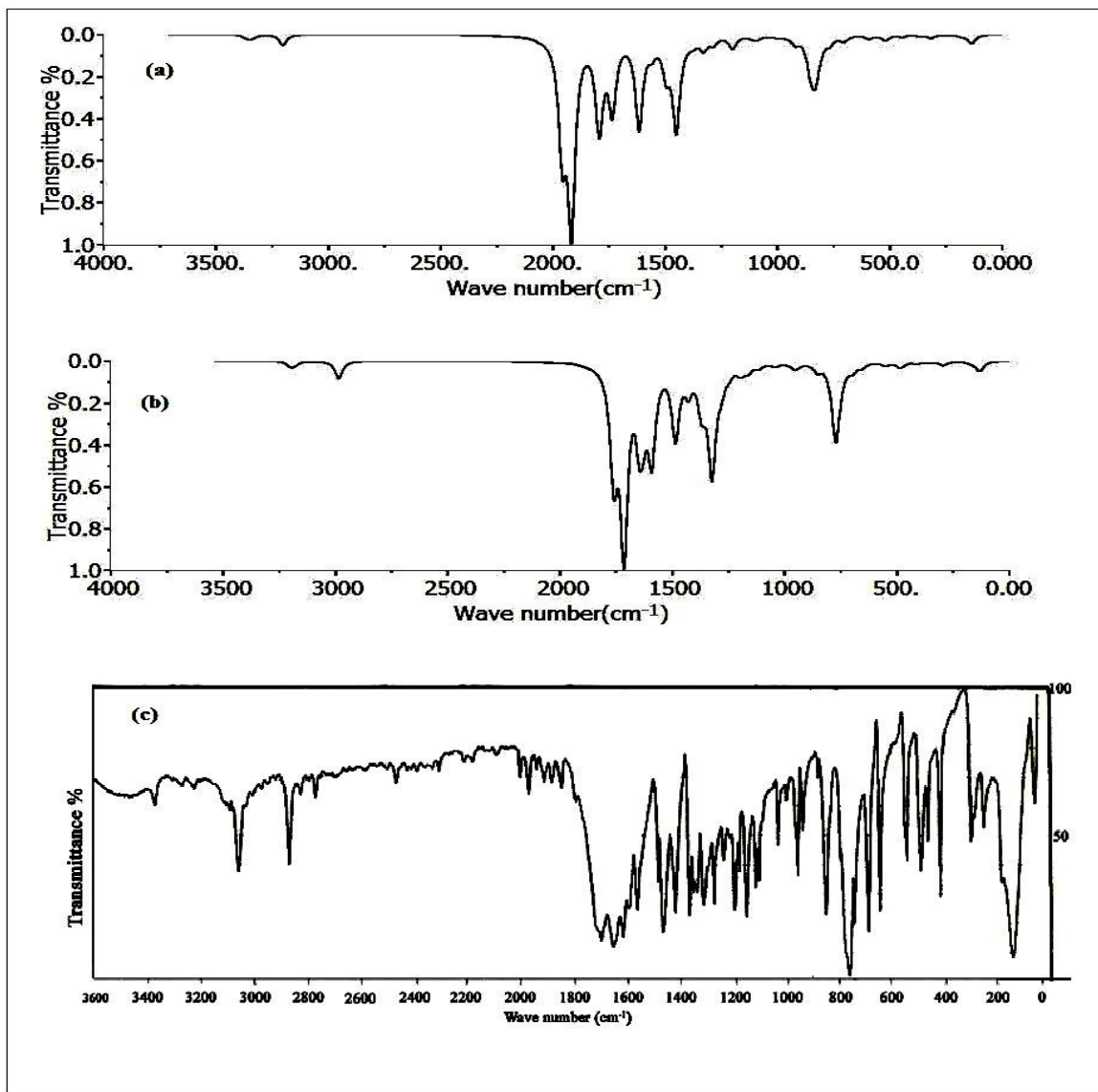


Fig. 2: FT-IR spectra of 3FC - (a) Theoretical with HF/6-311G++ (d, p), (b) Theoretical with B3LYP/6-311G++ (d, p), (c) Experimental.

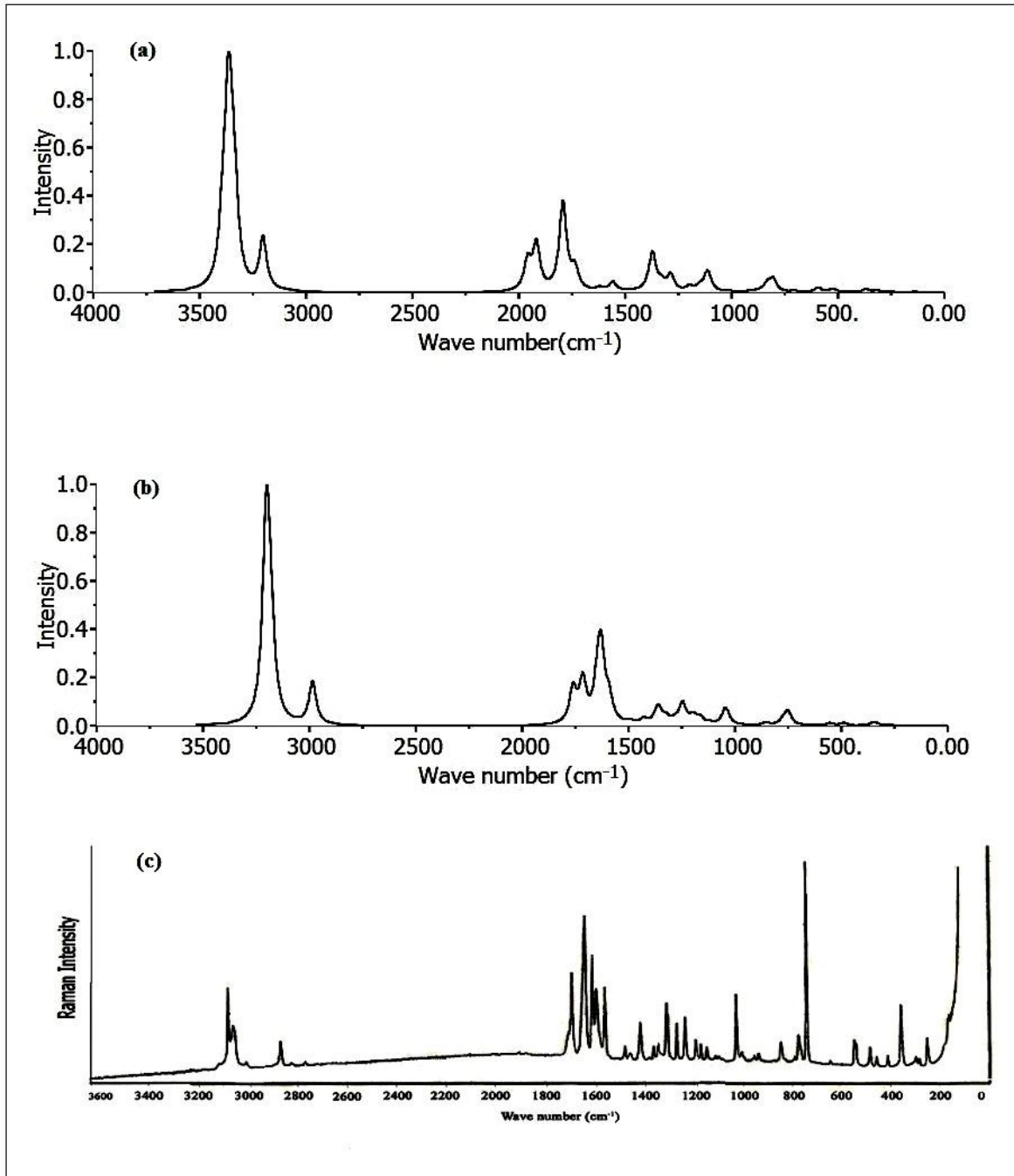


Fig. 3: FT-Raman spectra of 3FC - (a) Theoretical with HF/6-311G++ (d, p), (b) Theoretical with B3LYP/6-311G++ (d, p), (c) Experimental.

## RESULTS AND DISCUSSION

### *Analysis of Optimized geometry parameters*

From the optimized structure of the title compound by DFT method, The self-consistent field (SCF) energy is found to be relatively low (-610.4985 a.u) and all the theoretically computed wave numbers gives positive values, hence the optimized geometry is concluded as the most stable structure. The theoretically optimized structural parameters such as bond length and bond angle of the chosen molecule are compared with experimentally observed geometry of similar molecule such as 7-iodo-4-oxo-4H-chromene-3carbaldehyde<sup>11</sup>, 7,8-dichloro-4-oxo-4H-chromene-3 carbaldehyde<sup>12</sup>. Usually, in a six member ring, the bond length of C-O is 1.43 Å<sup>13</sup> but, in this study the bond length for C13-O16 and C3-O16 is 1.336 Å and 1.381 Å respectively. The reduction in the bond length is observed due to the fusion of benzene ring with pyrone ring through O16 atom<sup>14</sup>. The C9 = O15 and C17 = O19 bonds are confirmed by their respective distances of 1.224 Å, 1.2142 Å and it is seen that the bond parameter distortion is more in hetro ring compared to benzene ring. All the calculated C-H bond length is around 1.08 Å while the experimental value referred from the literature is 0.95 Å. The experimental values have been taken from X-ray diffraction method in solid phase, whereas the theoretical method is in the gas phase, therefore there is a deviation in C-H bond length. Generally, the difference in bond angle is characterized by the conjugation of the double bond, electro negativity and number of lone pair of electrons in a molecular system. The aldehyde group substitution affects the regular hexagonal structure of the ring, which is evident from the decrease in bond angle C12-C17-H18 (117.4°). The bond length, bond angle computed by HF/DFT methods are very close to the reported literature and which are collected in the Table 1.

### *Vibrational Analysis*

The Cartesian coordinates of the 19 atoms of the title molecule provides 51 internal modes and all the vibration modes are found to be active in both IR and Raman spectrum. Generally, for an N-atomic molecule, N-3 of all vibration is out of plane and 2N-3 is in plane. Thus, our molecules belonging to the Cs point group and 35 of all the 51 vibrations are in-plane and 16 modes is out-of plane. The experimental FTIR and FT-Raman wave numbers are usually lower than their quantum chemical calculation, therefore the root mean square difference in between the experimental and theoretical vibrational frequencies are minimized by using 0.97, 0.98, 0.99 multiple scaling factor and the wave numbers are matched with each other.

Table No. 1: “ Geometric parameters of the 3FC by HF and DFT methods with 6-311G++ (d, p) basis set”

Bond Length(A°)	HF	DFT	Ref [11]	Ref [12]	Bond Angle (in degree)	HF	DFT	Ref [11]	Ref [12]
C1- C2	1.375	1.387	1.387	1.387	C2- C1- C6	120.9	120.6	121.6	120.7
C1-C6	1.397	1.403	1.401	1.399	C2-C1-H7	119.4	119.4	118.6	120.0
C1- H7	1.075	1.084	0.950	0.950	C6-C1-H7	119.8	120.0	119.8	119.3
C2-C3	1.389	1.394	1.389	1.399	C1- C2- C3	118.6	118.6	117.7	118.3
C2-H8	1.074	1.083	0.950	0.950	C1- C2- H8	122.0	122.0	121.2	122.8
C3- C4	1.382	1.399	1.392	1.393	C3- C2- H8	119.4	119.4	121.2	118.8
C3-O16	1.360	1.381	1.386	1.374	C2- C3- C4	121.7	122.0	122.5	121.5
C4- C5	1.398	1.403	1.400	1.403	C2- C3- O16	116.7	116.5	115.5	116.2
C4- C9	1.481	1.483	1.471	1.479	C4-C3-O16	121.6	121.5	122.0	122.3
C5- C6	1.373	1.385	1.383	1.375	C3- C4- C5	118.7	118.2	118.2	119.0
C5- H10	1.074	1.083	0.950	0.950	C3-C4- C9	120.0	120.3	120.2	119.5
C6- H11	1.074	1.083	0.950	0.950	C5-C4-C9	121.4	121.4	121.5	121.6
C9- C12	1.468	1.470	1.462	1.452	C4- C5- C6	120.4	120.5	120.8	120.0
C9- O15	1.196	1.224	1.230	1.233	C4- C5-H10	118.1	117.7	119.6	119.9
C12- C13	1.338	1.356	1.355	1.349	C6-C5-H10	121.4	121.8	119.6	119.9
C12- C17	1.484	1.483	1.471	1.484	C1-C6- C5	119.7	120.0	119.1	120.4
C13- H14	1.073	1.083	0.950	0.950	C1- C6- H11	120.0	119.8	120.5	119.7
C13-O16	1.318	1.336	1.334	1.346	C5- C6- H11	120.3	120.1	120.5	119.8
C17 - H18	1.089	1.103	0.950	0.950	C4- C9-C12	113.6	113.8	113.9	114.2
C17- O19	1.188	1.214	1.222	1.207	C4- C9- O15	123.0	122.8	122.8	122.4
					C12- C9-O15	123.4	123.4	123.2	123.5
					C9 -C12-C13	120.0	120.4	120.5	120.8
					C9-C12-C17	120.9	120.7	120.1	120.9
					C13- C12-C17	119.2	119.0	119.4	120.9
					C12-C13-H14	122.2	122.5	117.4	117.7
					C12-C13-O16	125.1	125.1	125.1	124.5
					H14-C13-O16	112.7	112.4	117.4	117.7
					C3-O16-C13	119.7	119.0	118.2	118.3
					C12-C17-H18	114.9	114.4	118.0	118.1
					C12-C17-O19	123.5	123.9	123.9	123.8
					H18-C17-O19	121.6	121.7	118.0	118.1

For numbering of atom refer Fig. 1

The correlation graphs between the experimental and theoretical wave numbers at both HF and DFT methods are depicted in Fig.4. Gauss View (5.0) program<sup>15</sup> is employed to perform the theoretical vibrational frequency assignments with symmetry considerations. The experimentally observed and theoretically computed vibrational frequencies and the scaled frequencies and their respective vibrational assignments for the title molecule are shown in Table 2.

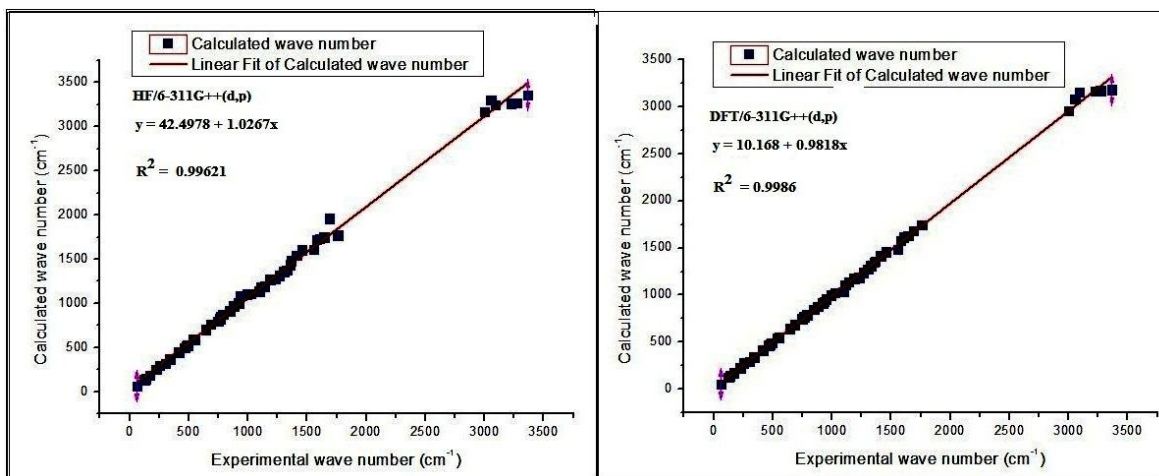


Fig.4: the correlation graphs between the experimental and theoretical wave numbers at both HF and DFT level.

### C-C Vibrations

In general, the aromatic skeletal ring (carbon-carbon stretching) vibrations appear in the region of  $1650\text{--}915\text{ cm}^{-1}$ <sup>16</sup>. In this study, the observed vibrational frequency at  $1643\text{ cm}^{-1}$  in FTIR,  $1639\text{ cm}^{-1}$  in FT-Raman are assigned to C-C stretching vibrations in benzene ring. The observed band  $1580\text{ cm}^{-1}$  at both in FTIR/FT-Raman and  $1606\text{ cm}^{-1}$  in FTIR,  $1610\text{ cm}^{-1}$  in FT-Raman have been assigned to C=C stretching vibrations in benzene and pyrone ring respectively. These vibrations are in good agreement with literature<sup>17</sup> and the calculated values. Prasad et al<sup>18</sup> reported that the C-C in-plane bending and out-of-plane bending vibrations lies in the region  $1000\text{--}400\text{ cm}^{-1}$ . In the present study, the characteristic absorption bands in FTIR spectrum at  $920, 746, 646$  and  $478\text{ cm}^{-1}$  and the bands in FT-Raman at  $762, 646$  and  $481\text{ cm}^{-1}$  were assigned to C-C-C in-plane bending and the out-of-plane bending vibrations are also observed at  $684, 463$  and  $415\text{ cm}^{-1}$  in FTIR and  $456, 415\text{ cm}^{-1}$  in FT-Raman spectrum.

### C-H Vibrations

In a heteroaromatic structure, the C-H stretching vibrations appear in the region  $2900\text{--}3150\text{ cm}^{-1}$  and the nature of the substituent are not appreciably affecting the vibration<sup>19</sup>. The investigated compound 3FC consists of a fused benzene and pyrone ring systems, in which the benzene ring gives rise to C-H stretching, C-H in-plane and out-of-plane bending. In the present study, the bands at  $3268, 3225, 3092$  and  $3051\text{ cm}^{-1}$  in FTIR and  $3080, 3052\text{ cm}^{-1}$  in FT-Raman were ascribed to C-H stretching vibration in benzene ring and the vibrational frequencies  $2999\text{ cm}^{-1}$  in FTIR and  $3033\text{ cm}^{-1}$  in FT-Raman were assigned to C-H stretching vibrations of aldehyde group. The C-H in plane and out-of-plane bending appears in the region  $1100\text{--}1500\text{ cm}^{-1}$  and  $600\text{--}900\text{ cm}^{-1}$  respectively<sup>20</sup>. At benzene ring, the bands observed at  $1303, 1230, 1188, 1143\text{ cm}^{-1}$  in FTIR and  $1310, 1235, 1178,$

1148, 1132  $\text{cm}^{-1}$  in FTR are assigned to C-H in - plane bending vibrations. The bands at 1411, 1329  $\text{cm}^{-1}$  in FTIR, and 1401 and 1326  $\text{cm}^{-1}$  in FTR are assigned to the C-H in - plane bending vibration at pyrone ring. In the aldehyde functional group of the title molecule, the C-H in-plane bandings are assigned to 1364, and 1356  $\text{cm}^{-1}$  in FTIR and 1347  $\text{cm}^{-1}$  in FTR spectrum. These assignments are in good agreement with the literature<sup>21</sup>. The C-H out- of plane bending is characterized at the bands 1026  $\text{cm}^{-1}$  in FTIR and 1029  $\text{cm}^{-1}$  in FTR at aldehyde group and 880, 790 768  $\text{cm}^{-1}$  in FTIR at benzene ring. These findings support assignments given in the literature<sup>22</sup>.

### C-O and C-CHO Vibrations

The characteristic frequency of C-O stretching vibration is absorbed in the range 1045  $\text{cm}^{-1}$ <sup>23</sup>. In this title compound, a strong carbonyl band of the pyrone ring and carboxylic acid band of the aldehyde are the two diverse type of stretching vibrations observed. The observed frequencies at 1132  $\text{cm}^{-1}$  in FTR and 1110, 1096  $\text{cm}^{-1}$  in FTIR are assigned to C-O stretching vibrations and this observation is in good agreement with literature<sup>24</sup>. The carbonyl group C=O stretching modes are appeared in the region from 1780 to 1700  $\text{cm}^{-1}$ <sup>25</sup>. For the title molecule, a very strong band at 1759  $\text{cm}^{-1}$  (in aldehyde group) and 1693, 1687  $\text{cm}^{-1}$  (in pyrone ring) are assigned to C = O stretching vibration. Here, the carbonyl group in the pyrone ring is part of a conjugated system, and the  $\pi$ -electron conjugation being localized. Hence, the wave number of the carbonyl stretching vibration (C=O) in the pyrone ring is lower than those of carbonyl group in aldehyde and these observed and theoretically calculated vibrational frequencies are in good agreement with the literature values<sup>26</sup>. In this molecular vibrational study, the characteristics of absorption bands observed at 933  $\text{cm}^{-1}$  in the FTIR and 927  $\text{cm}^{-1}$  in Raman are attributed to the C-CHO in-plane bending modes and out of plane bending modes are observed at 340, 358  $\text{cm}^{-1}$ . These assignments are in good agreement with the literature values<sup>27</sup>.

**Table No. 2: “Observed and calculated vibrational frequencies at HF and DFT with 6-311G++(d,p) basis sets of 3FC”**

Mode	Symmet	Experimental Frequencies ( $\text{Cm}^{-1}$ )		Calculated Frequencies ( $\text{Cm}^{-1}$ ) with 6-311G++(d,p) basis set				Vibrational Assignments
		FTIR	FTIR	HF Unscaled	DFT Unscaled	HF Scaled	DFT Scaled	
1	A'	3366vw		3395	3211	3361	3179	$\nu$ s (C-H) in pyrone ring
2	A'	3268vw		3371	3205	3270	3172	$\nu$ s (C-H) in benzene ring
3	A'	3225vw		3365	3201	3263	3168	$\nu$ s (C-H) in benzene ring
4	A'	3092vw	3080 s	3350	3190	3249	3157	$\nu$ s (C-H) in benzene ring
5	A'	3051 m	3052 w	3334	3177	3300	3081	$\nu$ s (C-H) in benzene ring
6	A'	2999 m	3033vw	3205	2988	3172	2958	$\nu$ s (C-H) from CHO
7	A'	1759 vs		1791	1763	1773	1745	$\nu$ s (C=O) from CHO

8	A'	1687 vs	1693 s	1981	1718	1960	1683	vs (C=O) pyrone ring
9	A'	1643 vs	1639 s	1769	1649	1751	1632	vs (C - C) in benzene ring
10	A'	1606 vs	1610 m	1753	1631	1735	1615	vs (C = C) in pyrone ring
11	A'	1580 s	1580 m	1739	1594	1721	1578	vs (C = C) in benzene
12	A'	1555 s	1560 m	1627	1499	1610	1484	vs (C= C) $\beta$ (C-H) in benzene
13	A'	1456 s	1466 s	1619	1489	1603	1459	vs (C- O)+vs (C=C)
14	A'	1411 s	1401 s	1561	1431	1545	1417	vs(O - C)+ $\beta$ (C- H) in pyrone
15	A'	1364 s		1499	1374	1483	1360	vs (C-CHO)+vs (C-C)
16	A'	1356 m	1347 s	1454	1361	1439	1347	vs (C-CHO)+ vs (C-C)
17	A'	1329 m	1326 s	1393	1326	1378	1312	vs(C- C)+ $\beta$ (C- H)
18	A'	1303 m	1310 s	1374	1285	1360	1272	vs (C- C)+ $\beta$ (C- H)
19	A'	1265 m	1256 s	1332	1249	1318	1236	vs(C- C)+v asy(C-O-C)
20	A'	1230 m	1235 s	1290	1201	1276	1188	vs(C- C)+v asy(C-O-C)
21	A'	1188 s	1178 m	1281	1187	1268	1174	$\beta$ (C - H)+ $\beta$ (C-O-C)
22	A''	1143 s	1148 m	1204	1166	1191	1142	$\beta$ (C- O - C)
23	A''	1110 m	1132 m	1198	1117	1186	1105	$\beta$ (C- O - C)
24	A''	1096 m		1151	1048	1139	1037	$\beta$ (O- C - C)
25	A''	1026 m	1029 m	1118	1033	1106	1023	$\beta$ (C- C- C)
26	A''	992 s		1115	1009	1104	999	(C- C- C) -Trigonal bending
27	A''	950 s		1099	985	1087	955	(C-C)- Ring breathing
28	A''	933 m	927 s	1093	960	1082	931	$\beta$ (C- CHO) + $\beta$ (C - H)
29	A''	920 m		1010	944	1000	916	$\beta$ (C- C- C) + $\gamma$ (C - H)
30	A''	880 vw		978	888	968	879	$\beta$ (C- C- C) + $\gamma$ (C - H)
31	A''	846 s	848 m	925	857	915	848	$\beta$ (C- C- C) + $\gamma$ (C - H)
32	A''	790 m		882	805	873	788	$\gamma$ (C - H)
33	A''	768 s		856	778	847	769	$\gamma$ (C - H)
34	A''	764 s	762 w	834	774	825	766	$\gamma$ (C - H)
35	A''	746 vs	742 vw	808	753	799	745	$\gamma$ (C - H)
36	A''	684 s		770	701	762	687	$\gamma$ (C - H)
37	A''	646 s	646 vw	708	659	700	645	$\gamma$ (C - H)
38	A''	553 m		596	556	590	550	$\gamma$ (H)(C = O)
39	A''	540 m	546 s	595	549	589	543	$\gamma$ (C -O -C)
40	A''	490 m		530	495	524	490	$\gamma$ (O - C -C)
41	A''	478 m	481 s	523	487	517	476	$\gamma$ (C- C - C)
42	A''	463 m	456 s	504	469	498	464	$\beta$ (C=O)
43	A''	415 m	415 s	449	415	444	415	$\gamma$ (C=O)
44	A''	340 s	358 w	373	349	368	342	$\gamma$ C-CHO
45	A''	301 s	298 m	320	297	316	294	$\gamma$ C-C-C
46	A''	253 m	252 vs	299	280	296	276	$\gamma$ C-C-C
47	A''	226 m		253	229	250	226	$\gamma$ C-C-C
48	A''	170 m		188	174	186	171	$\gamma$ C-C-C
49	A''	140 s		150	141	148	139	$\gamma$ C-C-C
50	A''	126 w		138	129	136	126	Lattice vibration
51	A''	62 s		63	57	62	56	Lattice vibration

vs-very strong, s-strong, m-medium, w-weak, vw-very weak,

vs - symmetric stretching, vas- asymmetric stretching,  $\beta$ - in-plane-bending,  $\gamma$  - out-of-plane bending.

### Frontier Molecular orbitals analysis

In general, the frontier molecular orbital HOMO and LUMO characterize the electron donating and accepting ability and the energy gap between HOMO and LUMO can be used to characterize the molecular chemical stability and interaction of the molecules with other species<sup>28,29</sup>. The plot of HOMO and LUMO for the title molecule is shown in Fig. 5. and the positive negative phases are represented in red and green colour. From the figure, The HOMO is localized over the C=C bond in the benzene ring but the LUMO is located over the oxygen atoms of the pyrone ring. Hence the HOMO → LUMO electron density transfer occurs from pyrone ring to aldehyde group.

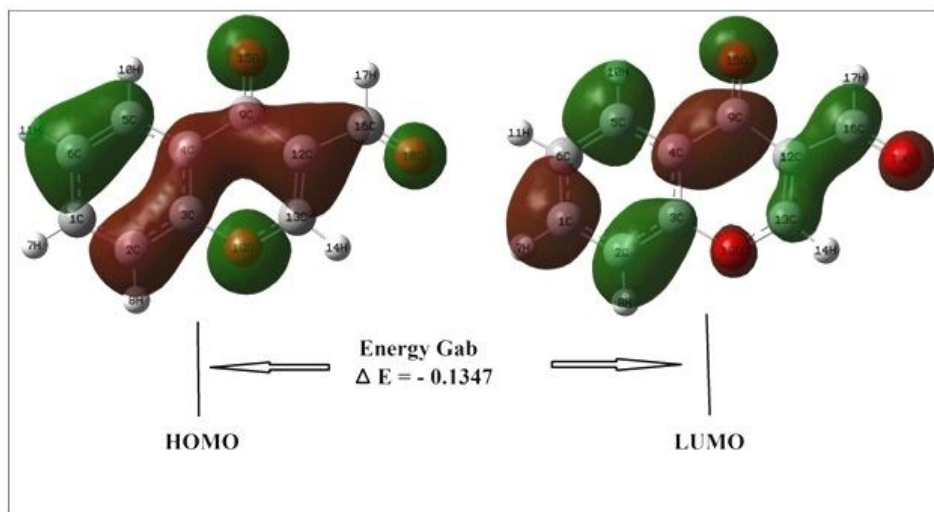
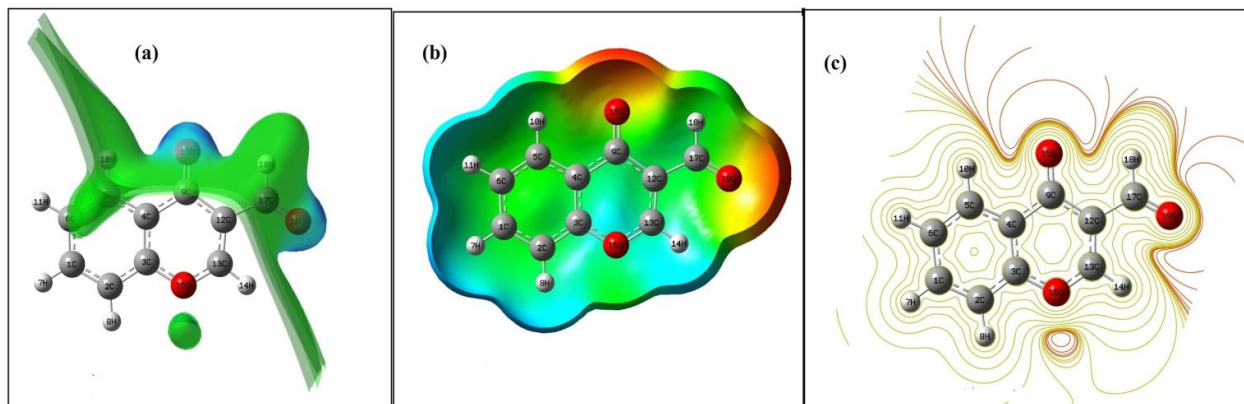


Fig. 5: Frontier molecular orbital's of 3FC

### Molecular Electrostatic Potential energy surface

The total electron density mapped with molecular electrostatic potential (MEP) surface is a very useful descriptor in understanding the nucleophilic, electrophilic reactive sites and hydrogen bonding interaction<sup>30</sup>. The total electron density and molecular electrostatic potential (MEP) surface has been plotted for the optimized geometry of the title compounds 3FC at the B3LYP/6-311++G (d,p) basis set. As can be seen from the MEP map of the investigated molecule, the blue region is the maximum positive region, which indicates the strongest attraction and preferred site for nucleophilic reactivity; hence the positive potentials are mapped over the nucleophilic reactive hydrogen atoms. The red and yellow colored regions are the negative potential regions which are preferred site for electrophilic reaction and mainly associated with lone pair of electro negative oxygen atoms O15 and O19 which shows a strongest repulsion in the molecule. From these results, lone pair of oxygen atoms O16 participated in the delocalization of ring  $\pi$  electron because of which O16 posses less negative charge when compared to O15 and O19. The green color covers C-C and C-H part of the title molecule where the potentials are close to zero. The accumulation of charge and depletion of the

charge is represented by dense and depletion region respectively. The observed contour map of the title molecule is as shown in Fig. 6.



**Fig.6: (a) Electrostatic Potential, (b) Molecular Electrostatic Potential and (c) Contour surface of the 3FC**

### *Natural Bonding Orbital (NBO) Analysis*

In the framework of molecular orbital theory of a molecular system, the interaction between the filled molecular orbital and unfilled (vacant) orbital can be expressed in terms of electron delocalization<sup>31</sup>. In the electron delocalization, the electron density is transferred from intra molecular donor orbital to acceptor orbital and the delocalization energy is estimated as the difference between the energy of the delocalized wave function and the energy of the reference wave function. The NBOs for a molecule system are calculated by a sequence transformation from Natural atomic orbital into Hybrid atomic orbital and Hybrid atomic orbital into Natural bond orbital. The wave function transformed into NBO form are in good agreement with Lewis structure and the covalence effects in molecules described by the strongly occupied NBOs of the natural Lewis structure<sup>32</sup>. In NBO analysis, a set of strongly occupied one centre like core, lone pair, two centre  $\pi$ ,  $\sigma$  bonds and a set of weakly occupied one centre Rydber, two centre  $\pi^*$ ,  $\sigma^*$  are generated. The strength of all the possible interaction between the strongly occupied Lewis type NBOs and weakly unoccupied non-Lewis type NBOs can be estimated from second-order perturbation theory analysis of the off-diagonal Fock matrix element which connects the two orbitals<sup>33</sup>. The second order perturbation analysis of Fock matrix of 3FC is tabulated in the Table 4, with different types of donor – acceptor interactions and their stabilization energy not less than 4.0 kcal mol<sup>-1</sup>. In the present study, A hyper-conjugative charge transfer occurs from the filled Lewis lone pair NBOs  $\pi$ C5 - C6 to the unfilled antibonding NBOs  $\pi^*$ C1 - C2 and  $\pi$ C1 - C2 to  $\pi^*$ C3 - C4 and the resulting stabilization energy are 22.04 and 21.49 Kcal mol<sup>-1</sup> respectively. The filled lone pair NBO nO15(2), exhibits a good overlap with unfilled antibonding NBOs  $\pi^*$ C12 - C13 with relatively high energy 20.83 Kcal

mol<sup>-1</sup>. From the table, it is seen that the maximum occupancies 1.99628, 1.99517 and 1.99024 are obtained for nO19 (2), σC12 - C17 and nO16 (2) respectively. Thus, the results obtained from NBO analysis provides convenient basis for investigating conjugative interactions or intra molecular charge transfer in molecular systems.

**Table No. 3: “Lists the selected values of the calculated second order interaction energy (E<sub>2</sub>) between donor-acceptor orbitals”**

Donor (i)	Occupancy	Acceptor(j)	Occupancy	E <sup>2</sup> Kcal mol <sup>-1</sup>	E <sub>j</sub> – E <sub>i</sub> (a.u)	F(i ,j) (a.u)
σ C1 – C2	1.97421	σ *C3 – O15	0.01299	4.89	0.94	0.061
π C1 – C2	1.67098	π* C3 – C4	0.31288	<b>21.49</b>	0.27	0.07
π C1 – C2	1.9811	π* C5 – C6	0.01545	17.27	0.29	0.064
σ C2 - C3	1.98054	σ* C3 - C4	0.01188	4.04	1.27	0.064
π C3 - C4	1.97654	π*C1 - C2	0.02017	17.11	0.29	0.064
π C3 - C4	1.97777	π*C5 - C6	0.01196	18.7	0.3	0.068
π C3 - C4	1.97556	π*C9 - O16	0.03044	18.09	0.28	0.066
σ C4 - C5	1.63627	σ*C3 - C4	0.41191	4.32	1.26	0.066
σ C4 - C5	1.98753	σ*C3 - O15	0.03567	4.33	0.95	0.057
π C5 - C6	1.97028	π* C1 - C2	0.01972	<b>22.04</b>	0.27	0.07
π C5 - C6	1.97574	π* C3 - C4	0.06478	20.16	0.27	0.067
σ C5 - H10	1.97946	σ* C3 - C4	0.01371	4.58	1.08	0.063
π C 9 - O16	1.65691	π* C3 - C4	0.2825	4.38	0.37	0.04
π C9 - O16	1.97785	π* C12 - C13	0.01274	4.94	0.37	0.039
π C12 - C13	1.98103	π*C9 - O16	0.01265	18.85	0.3	0.068
π C12 - C13	1.97858	π * C17 - O19	0.06178	14.92	0.29	0.06
σ C12 - C17	<b>1.99517</b>	σ*C13 - O15	0.0072	4.45	0.88	0.056
σ C13 - H14	1.96908	σ* C9 - C12	0.21582	5.16	0.97	0.064
π C17 - O19	1.98717	π*C12 - C13	0.0167	4.31	0.38	0.037
n O15 (1)	1.81687	σ* C3 - C4	0.14746	4.71	1.15	0.066
n O15(2)	1.97846	π*C3 - C4	0.05836	17.81	0.37	0.077
n O15 (2)	1.98101	π*C12 - C13	0.01624	<b>20.83</b>	0.37	0.079
n O16(2)	1.98745	σ*C4 - C9	0.02136	17.64	0.66	0.097
n O16(2)	<b>1.99024</b>	σ*C9 - C12	0.04107	17.81	0.65	0.097
nO 19(2)	<b>1.99628</b>	σ*C12 - C17	0.00228	17.22	0.63	0.094
n O19(2)	1.9827	σ* C17 - H18	0.0872	15.57	0.69	0.094

## The Mulliken population analysis

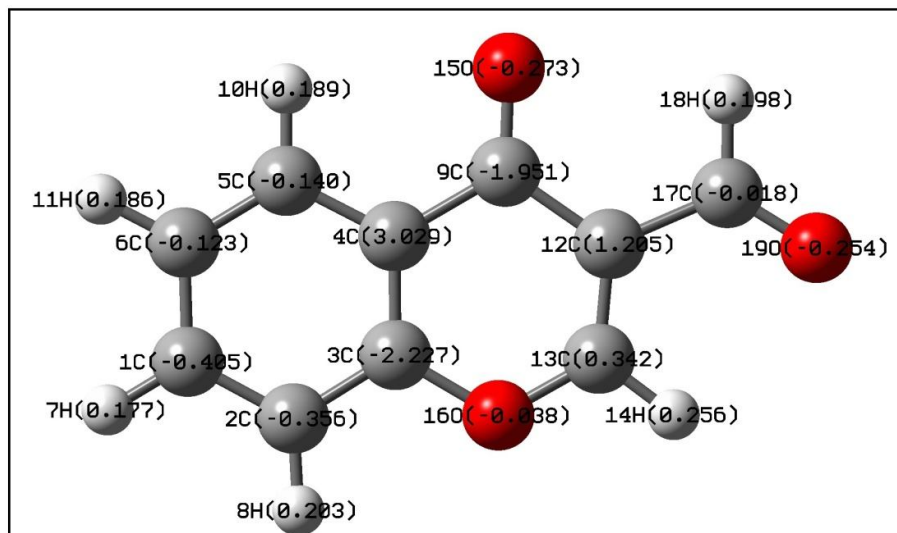


Fig. 7: Mulliken atomic charges of 3FC.

Atomic charge distributions in a molecular system play a vital role in computational chemistry and have strong relations to the biological activity<sup>34</sup>. The charges computed by Mulliken population analysis employing different methods but with same basis sets are not identical and in addition even with the same method but using different basis sets cannot be correlated. The Mulliken population analysis of the 3FC is carried out by employing HF and DFT methods using the same basis set 6-311++G (d,p). The electron distribution in the title molecule using DFT method are depicted in the Fig.7 and the Table 5 shows the comparison of Mullikan charge with natural atomic charges. The Mulliken atomic charges suggest the preferred position of nucleophilic attack and another interesting point from the population analysis is that the influence of the electronegative oxygen atoms O15, O16 and O19 makes the hydrogen atoms H14 and H18 to possess high electropositive charge and this may be mainly due to the fact that these hydrogen atoms are flanked by oxygen atoms in the molecular structure of 3FC.

### Thermodynamic Properties

By considering the title molecule as an asymmetric top and its rotational symmetry number as unity, the thermodynamic parameters such as entropy, enthalpy, internal energy, heat capacity, were calculated in gas phase using Moltran v.2.5<sup>35</sup> and are framed in Table 4. The correlation graphs between thermodynamic parameters and the temperatures (100–1000 K) are shown in Fig.8. It is worth mentioning that, the thermodynamic functions change shows that the molecule possesses more flexibility for changing its own thermodynamic system with respect to the temperature. The standard thermodynamic functions increase for all temperature from 100 to 1000 K, due to the increase of the intensities of molecular vibration as temperature increases<sup>36</sup>. In accordance with relationships of thermodynamic functions, these standard thermodynamic functions used to estimate directions of chemical reactions in thermo chemical field<sup>37</sup>.

**Table No. 4:** “Thermodynamic properties at different temperatures at the B3LYP/6-311++G(d,p) level for 3FC”

Temp. (K)	CV (J/K/mol)	CP (J/K/mol)	Internal Energy (kJ/mol)	Enthalpy (kJ/mol)	Entropy (J/K/mol)
100	62.172	70.486	361.915	362.746	289.932
200	109.615	117.929	370.474	372.137	353.144
298.15	158.64	166.95	383.64	386.12	409.36
300	159.55	167.865	383.932	386.427	410.399
400	206.168	214.483	402.27	405.596	465.223
500	245.401	253.715	424.915	429.072	517.447
600	276.98	285.30	451.09	456.08	566.60
700	302.24	310.55	480.10	485.92	612.55
800	322.62	330.93	511.38	518.03	655.40
900	339.28	347.59	544.50	551.98	695.37
1000	353.06	361.38	579.14	587.45	732.73

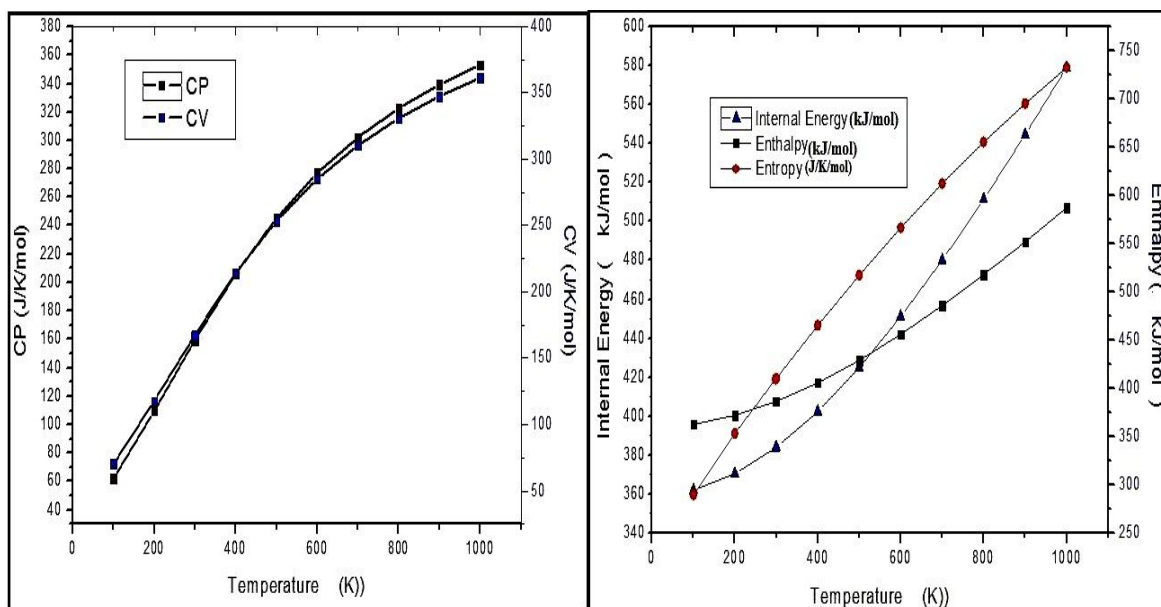


Fig.8: the correlation graphs between thermodynamic parameters and the temperatures

### Drug-Likeness and Bioactivity Scores

As a part of this study, Molinspiration<sup>38</sup> version 2016.10 validate the Lipinski's rule<sup>39</sup> (Rule of Five) and bioactivity score of the title compounds by predicting pharmaceutical molecular properties such as molecular volume, molecular weight, H-bond acceptors, H-bond donors, and logP (octanol/ water) to evaluate the drug likeness of the compounds. It can be noted from the Table .8 that the compound 3FC shows good drug likeness score and fulfills Lipinski's rule, which means that the titled molecule shows good permeability across cell membrane. Few more important pharmacokinetic parameters such as Topological polar surface area (TPSA) and number of rotatable bonds are introduced by Veber *et al*<sup>40</sup> to facilitate the identification of active lead compounds for drug bioavailability. These parameters are also computed for the title molecule and reported in Table-8. For a good drug, the TPSA value is 140 Å<sup>2</sup> or less expected to exhibit poor intestinal absorption and the rotatable bonds is less than 10 may have problems with bioavailability<sup>41</sup>. The TPSA and rotatable bonds of the title molecule is 47.28 Å<sup>2</sup> and 1 respectively. Thus, the investigated compound is expected to have good intestinal absorption. The bioactivity score of title compound including GPCR ligand, ion channel modulator, kinase inhibitor and nuclear receptor ligand are reported in Table.5. A molecule exhibits considerable bioactivity and when the bioactivity scores more than 0.00. The bioactivity score is -5.00 to 0.00 and is predicted to be in the moderate activity and is less than -5.00 is exhibits to be inactive<sup>42</sup>. The bioactive scores of the title molecule indicates that the molecule has moderate bioactivity and its score is comparable with that of the coumarin

which is having close structural similarity with the 3FC, and known to possess good therapeutic properties<sup>43</sup>.

Table No. 5: "Drug-Likeness and bioactivity Scores of 3FC"

Drug likeness score	3FC	Coumarin	Bioactivity score	3FC	coumarin
<u>miLogP</u>	1.54	2.01	GPCR ligand	-1.03	-1.44
<u>TPSA</u>	47.28	30.21	Ion channel modulator	-0.88	-0.86
natoms	13	11	Kinase inhibitor	-1.06	-1.57
nON	3	2	Nuclear receptor ligand	-0.91	-1.42
nOHNH	0	0	Protease inhibitor	-1.64	-1.43
nviolations	0	0	Enzyme inhibitor	-0.36	-0.58
nrotb	1	0			
volume	147.57	<b>128.59</b>			
MW	174.16	<b>146.15</b>			

Logarithm of partition coefficient between n-octanol and water (miLogP). Topological polar surface area (TPSA). Total number of atoms (natoms). Number of hydrogen bond acceptors (n-ON). Number of hydrogen bond donors (n-OHNH). Number of rotatable bonds (n-rotb). Molecular weight (MW) and volume.

### ***Molecular Docking Study***

In the structure based drug design, molecular docking is a one of the most recurrently used methods because of its ability to sense the best conformation of ligand molecule which is small and is within the appropriate target site of the protein structure<sup>44-45</sup>. In this molecular docking study, the target protein is kept rigid and the ligand molecule is allowed to act flexibly. There are three proteins were selected as the protein target such as the p38delta (PDB ID: 3coi), Human NAD(P)H-quinone oxidoreductase (PDB ID: 1gg5) and Human NAA50 cell line (PDB ID: 4x5k). The p38delta is a member of the mitogen activated protein kinase, which is involved in promoting cell promoting proliferation and tumor development in the outer layer of the skin and may possess therapeutic implication for skin cancer. NAD (P) H: quinone oxidoreductase 1 (NQO1) is a flavo-enzyme, which plays a vital role in shielding the cell from oxidative stresses<sup>46</sup> highly found in diverse epithelial cells, vascular endothelium, adipocytes<sup>47</sup> and in many human solid tumours<sup>48-49</sup>. The molecular geometry of the title compound ligand (3FC), is optimized and energies is minimized with the density functional theory (DFT) at the B3LYP/6-311G++ (d,p) level using Gaussian 09 program. For all the three target protein 3coi, 1gg5 and 4x5k, atomic charges are calculated by Kollman method and polar hydrogen atoms are added to the protein, co-crystallized ligands and the water molecules

are removed. In Auto Dock, ten runs are performed for each target proteins and the best conformation is chosen with the lowest binding energy after completing the docking search. The lowest binding energy for the best poses is taken as the final binding affinity value and the interaction between the different targets proteins with title compound are analyzed using Discover Studio Visualizer 4.0. The docking pose of the 3FC with the target protein and their interactions are shown in the Figure 9, 10,11 and 12 and the docking results are summarized in the Table 6. The binding energy value and the H-bonds are obtained in the present docking study confirm that inhibition may be specific to those sites where oxygen atom is present and all these interactions stabilize the inhibitor substrate of protein - ligand complex. This virtual screening study validate that the title compound 3FC have a better interaction with Human NAA50 cell line with more number of hydrogen bonds due to the existence of a formyl group at the C-3 position. The docking pose of the 3FC with the Human NAA50 cell line is as shown in Figure 8 and 9. The existence of an unsaturated reactive aldehyde at the C-3 position can react as acceptor and it seems to be accountable for various biological activities<sup>50</sup>.

**Table No. 6: “The predicted binding energies and H-bond analysis”**

Name of the Target protein	Binding Energy (BE) kcal/mol	Estimated Inhibition constant (Ki) uM	Binding site residues	Donor atom	Acceptor atom	H- Bond Distance (Å)	$\pi$ - $\pi$ Residue
3coi	-4.69	364.37	TRP89	NE1	O	2.893	GLU A:33
			ARG82	NE	O	2.843	
			ARG82	NH2	O	3.090	
1gg5	-6.31	23.55	VAL A:108	N	O	3.104	PHE A:123
			VAL C:108	N	O	3.073	
			LYS C:113	NZ	O	2.881	
4x5k	-6.62	14.13	THR90	OG1	O	2.879	PHE A:123
			ILE88	N	O	2.978	
			GLY87	N	O	3.085	

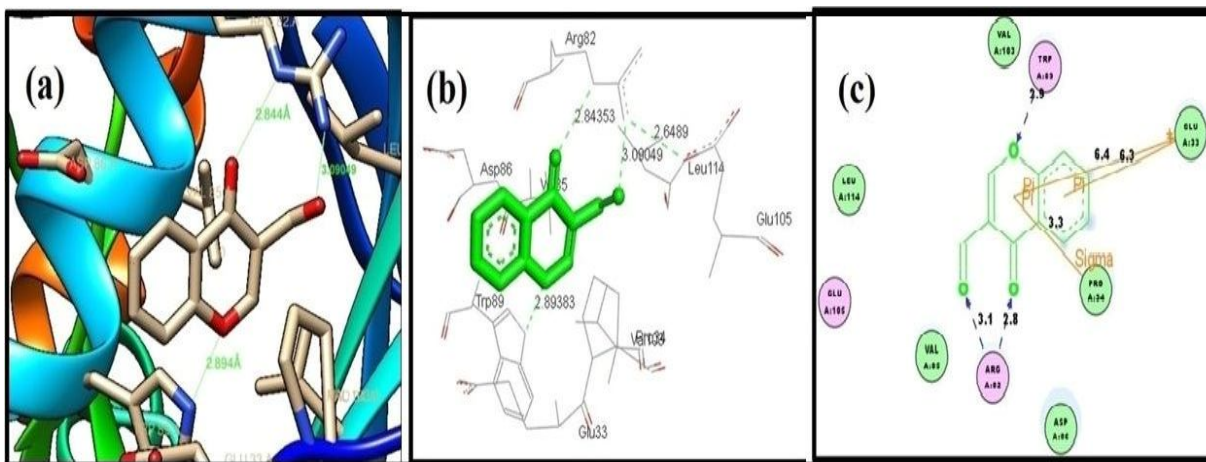


Fig.9: Docked orientation of 3FC with target protein( PDB ID : 3coi). (a) & (b) are three-dimensional Structural views and (c) is the two -dimensional structural views.

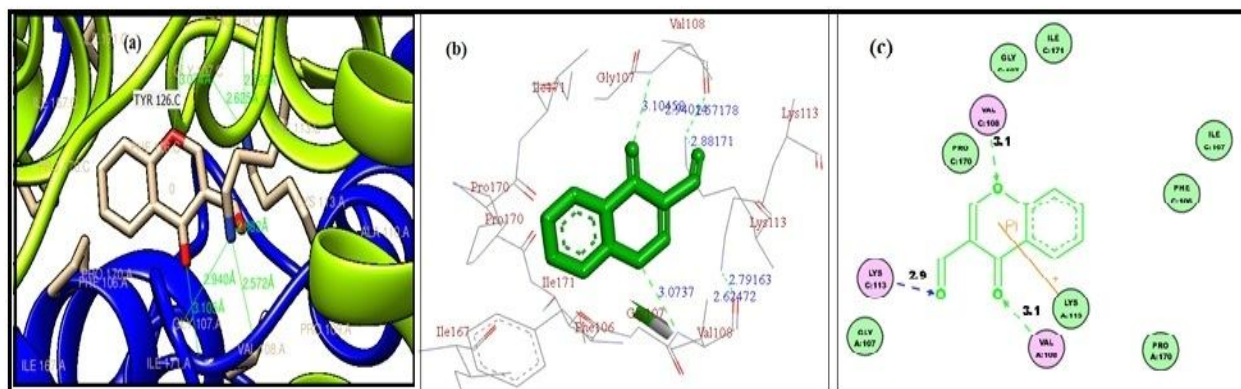


Fig. 10: Docked orientation of 3FC with target protein (PDB ID: 1gg5). (a) & (b) are three-dimensional Structural views and (c) is the two -dimensional structural views.

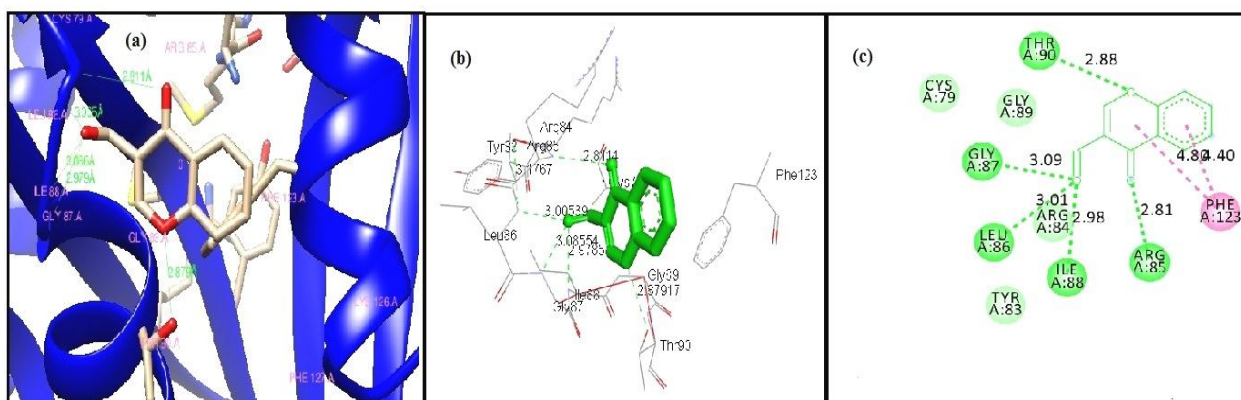


Fig. 11: Docked orientation of 3FC with target protein (PDB ID: 4x5k). (a) & (b) are three-dimensional Structural views and (c) is the two -dimensional structural views.

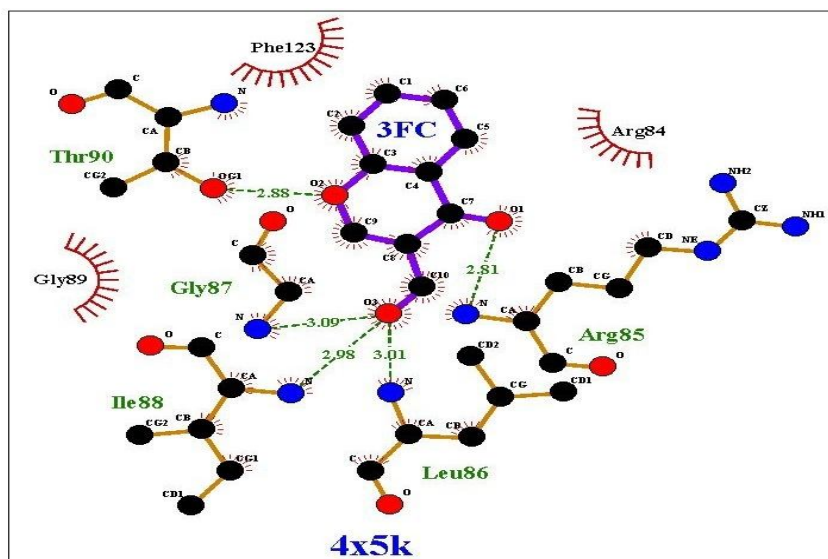


Fig. 12: The docking pose of the 3FC with the Human NAA50 cell line (PDB: 4x5k)

## CONCLUSION

In this study, the FT-IR and FT-Raman spectra of the 3FC are recorded experimentally and is theoretically simulated by employing HF and DFT methods utilizing 6-311++G (d,p) basis sets from the optimized molecular structure. The calculated vibrational frequency values are scaled to rationalize the observed values and the complete assignments are proposed for the first time. The charge transfer interaction within the molecule are analyzed by carrying out FMO analysis which shows that the electron density transfer occurs from pyrone ring to aldehyde group. By mapping the molecular electrostatic potential, the possible sites of nucleophilic attacks in the molecule are identified as sites where an oxygen atom is present. The thermo chemistry data for the titled compound are computed and the variation of entropy, enthalpy and specific heat capacity with temperature are also presented. The pharmaceutical molecular properties such as drug bioavailability, drug likeness of the chosen compounds are studied and compared with similar drug. The titled molecule obeys the Lipinski rule and indicates that the chosen molecule is a better drug candidate. The biological activity of the titled compound can be understood by molecular docking study. The docking analyses indicated that the title compound interact mainly with residues TRP 89 A, ARG 82A, THR 90A, LEU 86A, GLY87 A, ILE88A, GLUA 33, PRO A34, PHE123A by making hydrogen bonds and  $\pi$ - $\pi$ ,  $\pi$ - $\sigma$  interactions. This molecular docking study is also shows that the molecule 3FC docks better with residues of the Human NAA50 cell line and hence can be used to treat diseases affecting this protein.

## REFERENCE

1. Machado NFL, Marques MPM, Bioactive Chromone Derivatives- Structural Diversity, *Curr Bioact Compd.* 2010; 6(2):76–89.
2. Harborne JB, Williams CA, *Advances in Flavonoid research since 1992*, *Phytochemistry*.2000; 55: 481.
3. Meenu Beniwal, Neelam Jain, Review Article on Vilsmeier Haack Reaction and Its Applications, *ejbps.* 2015; 2:1340-1374.
4. Ghosh CK, Chakraborty A, *Chemistry and Application of 4-Oxo-4h-1benzopyran-3-Carbox aldehyde.* , 2015; *Arkivoc (Vi)*: 288-361.
5. Magdy Ahmed Ibrahim, Tarik El-SayedAli Nasser Mohamed El-Gohary an Azza MohamedEl-Kazak, 3-Formylchromones as diverse building blocks in heterocycles synthesis, *European Journal of Chemistry.* 2013; 4(3): 311-328.
6. Agnieszka Dzielulska-Kulaczowska, Liliana Mazur, Structural studies and characterization of 3-formylchromone and products of its reactions with chosen primary aromatic amines, *J.Mol.Struct.* 2011; 985: 233–242.
7. Frisch M-J, Trucks G-W, Schlegel H-B, Scuseria G-E, Robb M-A, Cheeseman J-R, Montgomery J-A Jr, Vreven T, Kudin K-N, Burant J-C, Millam J-M, Iyengar S-S, Tomasi J, Barone V, Mennucci B, Cossi M, Scalmani G, Rega N, Petersson G-A, Nakatsuji H, Hada M, Ehara M, Toyota K, Fukuda R, Hasegawa J, Ishida M, Nakajima T, Honda Y, Kitao O, Nakai H, Klene M, Li X, Knox J-E, Hratchian H-P, Cross J-B, Bakken V, Adamo C, Jaramillo J, Gomperts R, Stratmann R-E, Yazyev O, Austin A-J, Cammi R, Pomelli C, Ochterski J-W, Ayala P-Y, Morokuma K, Voth G-A, Salvador P, Dannenberg J-J, Zakrzewski V-G, Dapprich S, Daniels A-D, Strain M-C, Farkas O, Malick D-K, Rabuck A-D, Raghavachari K, Foresman J-B, Ortiz J-V, Cui Q, Baboul A-G, Cli@ord S, Cioslowski J, Stefanov B-B, Liu G, Liashenko A, Piskorz P, Komaromi I, Martin R-L, Fox D-J, Keith T, Al-Laham M-A, Peng C-Y, Nanayakkara A, Challacombe M, Gill P-M-M, Johnson B, Chen W, Wong M-W, Gonzalez C, Pople J-A, *Gaussian 09, Revision A 02* Gaussian Inc Wallingford CT, 2009.
8. Allouche AR, A graphical user interface for computational chemistry softwares, *Journal of Computational Chemistry.* 2011; 32: 174–182.
9. Scott AP, Random L, Harmonic Vibrational Frequencies: An Evaluation of Hartree-Fock, Moller-Plesset, Quadratic Configuration Interaction, Density Functional Theory and Semiempirical Scale Factor, *J Phys Chem.* 1996; 100: 16502-16504.
10. Huey R, Morris GM, *Using AutoDock 4 with AutoDocktools: a tutorial.* La Jolla, CA, USA, *The Scripps Research Institute, Molecular Graphics Laboratory*, 2008; 54-56
11. Yoshinobu Ishikawa, Crystal structure of 7-iodo-4-oxo-4H-chromene-3carbaldehyde, *Acta Cryst.* 2016; E72:1724–1727.
12. Yoshinobu Ishikawa, Crystal structure of 7,8-dichloro-4-oxo-4H-chromene-3-carbaldehyde, *Acta Cryst.* 2015; E71: 902–905.
13. Arjunan V, Sakiladevi S, Marchewka MK, Mohan S, FTIR, FT-Raman, FT-NMR and quantum chemical investigations of 3-acetylcoumarin, *Spectrochim. Acta.* 2013; 109: 79-89.
14. Prabavathi N and Senthil Nayaki N , Molecular structure, FT-IR, FT-Raman, NMR studies and first order molecular hyperpolarizabilities of 7methoxy-4-methylcoumarin by DFT Method, *Phys.Express.* 2014; 4(12):1-15.
15. Frisch A, Neilson A-B, Holder A-J, *GAUSSVIEW user Manual* Gaussian Inc Pittsburgh CT, 2009.
16. G. Varsanyi, *Assignments for Vibrational Spectra of Seven Hundred Benzene Derivatives*, Wiley, New York, 1974.
17. IrenaKostova, Tsvetanka stefanova., New gallium(III) complex synthesis,spectral characterization and cytotoxicity, *Indian J. Pure Appl. Phys.* 2012; 50: 547-554.

18. Prasad MVS, Kadali Chaitanya, Udaya Sri N. and Veeraiah V, Experimental and theoretical (HOMO, LUMO, NBO analysis and NLO properties) study of 7-hydroxy-4-phenyl coumarin and 5, 7-dihydroxy-4-phenylcoumarin, *J.Mol.Struct.* 2013; 1047:216–228.
19. Krishnakumar V, John Xavier R, Normal coordinate analysis of 2-mercapto and 4,6-dihydroxy - 2-mercapto pyrimidines, *Indian J. Pure Appl. Phys.* 2003; 41(8): 597–601.
20. Kavitha E, Sundaraganesan N, and Sebastian S, Molecular structure, vibrational spectroscopic and HOMO-LUMO studies of 4- nitroaniline by density functional method, *Indian J. Pure & App. Phy.* 2010; 48: 20–30.
21. Pavia DI, Lampman GM and Kriz GS, Introduction to spectroscopy: A guide for student of organic chemistry, Physics, in: J. Vondeling (Ed.), third ed., Thomson, Learning, 2001.
22. Jamelah S, Al-Otaibi, Tautomerization, molecular structure, transition state structure, and vibrational spectra of 2-aminopyridines: a combined computational and experimental study, *Al-Otaibi SpringerPlus.* 2015; 4:586.
23. Panicker CY, Varghese HT, Raj A, Raju K, Bolelli TE, et al, IR, Raman and SERS spectra of 2-phenoxyethylbenzothiazole, *Spectrochim Acta.* 2009;74:132–139.
24. Roeges NPG, *A Guide to the Complete Interpretation of Infrared Spectra of Organic Structures*, Wiley, New York, USA, 1994.
25. B. Smith, *Infrared Spectral Interpretation, a Systematic Approach*, CRC Press Washington, DC, 1999.
26. Mukherjee M, Misra TN, Surface-Enhanced Raman Spectra of 2- and 3-Hydroxypyridines in Silver Sol, *J. Raman. Spectrosc.* 1996; 27: 595-600.
27. Margita Lacova, Dusan Loos, Mikulas Furdik, Maria Matulova, Hafez M. El-Shaer, Synthesis and Reactions of New 4-Oxo-4H-benzopyran-3-carboxaldehydes Containing Hydroxy Groups or 2-Oxopyran Cycles, *Molecules.* 1998; 3: 149–158.
28. Mehmet Karabacak, Mehmet Cinar, Mustafa Kurt, Molecular structure and vibrational assignments of hippuric acid: A detailed density functional theoretical study, *Spectrochim. Acta Part A, Mol. Biomol. Spectrosc.* 2009; 74:1197–1203.
29. Ditchfield R, *Mol. Phy* 1974; 27: 789–807.
30. Peter Politzer, Jane Murray S, *Concepts and Methods in Modern Theoretical Chemistry*, CRC Press, 143-180, 2013.
31. Reed AE, Weinhold F, Natural Localized Molecular Orbitals, *J. Chem. Phys.* 1985; 83:1736-1740.
32. Reed AE, Curtiss LA, Weinhold F, Intermolecular Interaction from a Natural Bond Orbital, Donor-Acceptor Viewpoint, *Chem.Rev* 88: 899-926, 1988.
33. Weinhold F, Landis CR, *Valency and Bonding: A Natural Bond Orbital Donor- Acceptor Perspective*, Cambridge, Cambridge University Press, 2005.
34. Mahmoud S. Said and Zaheda A, Najim A Theoretical Approach to Relate the Reactivity Descriptors and Mulliken Charges with Carcinogenicity of Some Methylated Benzo[a]Anthracene, *Pak. J. Anal. Environ. Chem.* 2005;13, 1, 40-47.
35. Ignatov SK, MOLTRAN v.2.5, Program for Molecular Visualization and Thermodynamic Calculations, University of Nizhny Novgorod, Nizhny Novgorod, Russia, 2007.
36. Bevan Ott J, Boerio-goates J, *Calculations from Statistical Thermodynamics*, Academic Press, 2000.
37. Zhang R, Dub B, Sun G, Sun Y, Experimental and theoretical studies on o-, m- and p-chlorobenzylideneaminoantipyridines, *Spectrochim. Acta A.* 2010; 75: 1115–1124.
38. Molinspiration Cheminformatics, Bratislava, Slovak Republic, <http://www.molinspiration.com>.
39. Lipinski CA, Lombardo F, Dominy BW and Feeney PJ, Experimental and computational approaches to estimate solubility and permeability in drug discovery and development settings, *Adv. Drug Del. Rev.* 2002; 23:4–25.

40. Veber DF, Johnson SR, Cheng HY, Smith BR, Ward KW, Kopple KD. Molecular properties that influence the oral bioavailability of drug candidates. *J. Med. Chem.* 2002; 45: 2615-2623.
  41. Ertl P, Rohde B and Selzer P, Fast calculation of molecular polar surface area as a sum of fragment- based contributions and its application to the prediction of drug transport properties, *J. Med. Chem.* 2000; 43(20): 3714-7.
  42. Singh S, Gupta AK, Verma A, Molecular properties and bioactivity score of Aloe vera antioxidant compounds-in order to lead finding, *Res J Pharm Biol Chem Sci.* 2013; 4(2): 876-81.
  43. Borges F, Roleira F, Milhazes N, Santana L, Uriarte E, Simple Coumarins and Analogues in Medicinal Chemistry: Occurrence, Synthesis and Biological Activity, *Current Medicinal Chemistry.* 2005; 12:887-916.
  44. López-Vallejo F, Caulfield T, Martínez-Mayorga K, Giulianotti MA, Houghten RA, Nefzi A, Medina-Franco JL, Integrating virtual screening and combinatorial chemistry for accelerated drug discovery, *Comb. Chem. High Throughput Screen.* 2011; 14: 475–487.
  45. Meng XY, Zhang HX, Mezei M, Cui M, Molecular docking: A powerful approach for structure-based drug discovery, *Curr. Comput. Aided Drug Des.* 2011; 7:146–157.
  46. Nebert DW, Roe AL, Dieter MZ, Solis WA, Yang Y, Dalton TP, Role of the aromatic hydrocarbon receptor and [Ah] gene battery in the oxidative stress response, cell cycle control, and apoptosis, *Biochem Pharmacol.* 2000; 59: 65–85.
  47. Siegel D, Ross D, Immunodetection of NAD(P)H:quinine oxidoreductase 1 (NQO1) in human tissues, *Free Radic Biol Med.* 2000; 29:246–53.
  48. Yang Y, Zhang Y, Wu Q, Cui X, Lin Z, Liu S1, Chen L, Clinical implications of high NQO1 expression in breast cancers. *J Exp Clin Cancer Res.* 2014; 33:14.
  49. Schlager JJ, Powis G, Cytosolic NAD(P)H:(quinoneacceptor)oxidoreductase in human normal and tumor tissue: effects of cigarette smoking and alcohol, *Int J Cancer.* 1990; 45:403–9.
  50. Masami Kawase, Toru Tanaka, Hiroyuki Kan, Satoru Tani, Hideki Nakashima, Hiroshi Sakagami, Biological Activity of 3-Formylchromones and Related Compounds, *In vivo.* 2007; 21: 829-834.
-